

# P3Nav: A Unified Framework for Embodied Navigation Integrating Perception, Planning, and Prediction

Yufeng Zhong\*   Chengjian Feng\*   Feng Yan   Fanfan Liu   Liming Zheng  
Lin Ma<sup>†</sup>  
Meituan Inc.

## Abstract

In language-guided visual navigation, agents locate target objects in unseen environments using natural language instructions. For reliable navigation in unfamiliar scenes, agents must possess strong perception, planning, and prediction capabilities. Additionally, when agents revisit previously explored areas during long-term navigation, they may retain irrelevant and redundant historical perceptions, leading to suboptimal results. In this work, we introduce **P3Nav**, a unified framework that integrates **Perception, Planning, and Prediction** capabilities through **Multitask Collaboration** on navigation and embodied question answering (EQA) tasks, thereby enhancing navigation performance. Furthermore, P3Nav employs an **Adaptive 3D-aware History Sampling** strategy to effectively and efficiently utilize historical observations. By leveraging the large language models (LLM), P3Nav comprehends diverse commands and complex visual scenes, resulting in appropriate navigation actions. P3Nav achieves a 75% success rate in object goal navigation on the CHORES-S benchmark, setting a new state-of-the-art performance.

## 1. Introduction

Embodied navigation [1], particularly language-guided visual navigation [3, 6, 11, 15, 16, 21–23] is essential for enabling robots to perform various tasks, presenting a significant challenge for researchers. Language-guided visual navigation requires agents to understand natural language instructions and autonomously navigate in unseen visual environments to locate target objects. To reliably navigate in unfamiliar visual environments, agents must effectively perceive surrounding scenes, plan strategies for reaching their goals, and predict appropriate navigation actions.

Recently, significant advancements in language-guided visual navigation have been driven by the robust under-

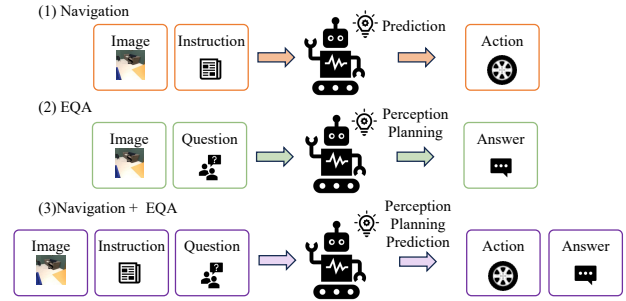


Figure 1. **Multitask collaboration.** In (1) navigation tasks, only actions are produced, missing the perception and planning found in (2) EQA tasks. (3) Multitask collaboration unifies perception, planning, and prediction for a more comprehensive model.

standing and generalization capabilities of visual-language models (VLMs) that seamlessly integrate visual and textual information. For example, in Object Goal Navigation (ObjectNav) [3–6, 8, 11, 21–23, 27, 33, 35], numerous approaches [4, 5, 8, 27, 33, 35] leveraging VLMs have achieved impressive results. These methods utilize VLMs to effectively interpret and align object categories with visual inputs, enabling agents to navigate toward specified objects with enhanced accuracy and efficiency. By combining visual and textual information, these approaches significantly enhance comprehension of complex environments and adaptation to new scenarios. While current navigation models excel at locating target objects, they often struggle to provide efficient path planning and to explain the reasoning behind their path choices, as shown in the *first row* of Fig. 1. This challenge is largely due to traditional navigation datasets focusing primarily on recording coordinate trajectories and neglecting the hierarchical reasoning process employed by humans. For instance, humans typically first identify rooms, then locate furniture, and finally search for specific objects.

Additionally, we have observed a significant amount of redundancy in observations during navigation, as agents frequently revisit the same locations multiple times. As illustrated at the *top* of Fig. 2, the white circle marks ar-

\*Equal contribution.

<sup>†</sup>Corresponding author.

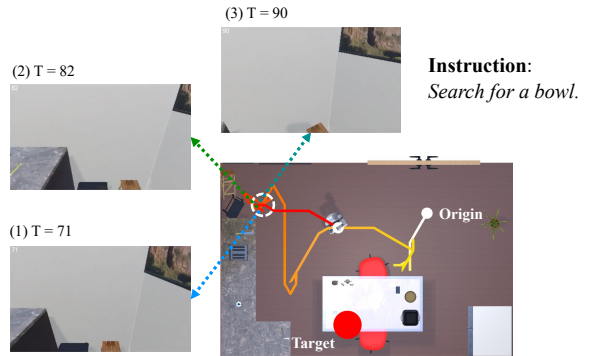
reas that the agent revisits multiple times. At (1)  $T = 71$  and (2)  $T = 82$ , the agent focuses on the countertop area and two chairs. At (3)  $T = 90$ , the scene remains largely unchanged, capturing an environment similar to that at (1) and (2) once again. These observations demonstrate that the scenes within the revisit areas are highly similar, highlighting the redundancy present in the agent’s perception. Therefore, when agents revisit the same area, previous observations may become redundant and should be discarded.

To address these limitations, we present **P3Nav**, a unified framework for embodied navigation that integrates **P**erception, **P**lanning, and **P**rediction. As shown in Fig. 1, we develop a **Multitask Collaboration** strategy that enables agents to leverage perception and planning to improve their prediction capabilities by conducting joint training on both navigation and embodied question answering (EQA) tasks. To achieve this, we have devised a novel method for constructing EQA datasets that explicitly model the decision-making process involved in navigation, with more details available in Sec. 3.2.

Furthermore, P3Nav employs an **Adaptive 3D-aware History Sampling** strategy to effectively and efficiently utilize historical observations in navigation. Specifically, this method selects RGB frames that do not overlap in spatial positions to serve as valid observations and introduces **position-enhanced historical features** that utilize the agent’s positions to augment historical semantic features with trajectory information, thereby preventing redundant exploration of the same location. As illustrated at the *bottom* of Fig. 2, we transform the dense and disorganized trajectory into sparse and organized steps, minimizing redundancy while preserving crucial observations at key locations. Finally, by leveraging the large language model (LLM), P3Nav can understand diverse instructions and complex visual scenes, resulting in effective navigation. Through extensive experimentation, P3Nav has demonstrated remarkable capabilities, achieving an impressive 75% success rate in ObjectNav on the CHORES-S benchmark [10]. This performance not only sets a new state-of-the-art but also represents a substantial 18% absolute improvement over previous methods.

The main contributions of this paper include: (1) We introduce **P3Nav**, a unified framework integrating **P**erception, **P**lanning, and **P**rediction, enhancing navigation by multitask collaboration on navigation and EQA tasks. (2) P3Nav employs the adaptive 3D-aware history sampling strategy, effectively utilizing historical observations by selecting non-overlapping RGB frames to reduce redundancy. (3) P3Nav achieves an 75% success rate in ObjectNav on the CHORES-S benchmark, setting a new state-of-the-art, with a 18% absolute improvement over previous methods.

### Revisit in Navigation



### Adaptive 3D-aware History Sampling

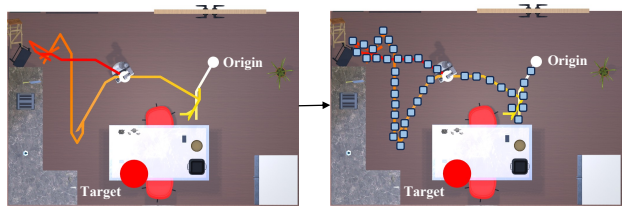


Figure 2. *Top*: During long-term navigation, agents may revisit the same areas multiple times, making previous observations redundant. For instance, at  $T = 71$ ,  $T = 82$ , and  $T = 90$ , the scenes observed are very similar, highlighting the redundancy in the agent’s perception. *Bottom*: Using the **Adaptive 3D-aware History Sampling** strategy, we transform the dense and disorganized trajectory into sparse and organized steps, reducing observational redundancy while preserving visual information at key locations. The trajectory is produced by the SPOC-driven agent [10].

## 2. Related Work

Embodied navigation [1] involves guiding agents through unseen environments based on human instructions. While the field includes various navigation paradigms, our research specifically focuses on multimodal tasks that combine visual perception with language processing. In this paper, we emphasize areas like ObjectNav [22] and EQA [7].

### 2.1. Object Goal Navigation

The research landscape of ObjectNav [22] can be systematically organized based on the scope of vocabulary and adaptability to real-world scenarios, classifying them into closed-world and open-world categories. In the closed-world category, traditional ObjectNav tasks [3–6, 8, 11, 18, 21, 23, 27, 33, 35] focus on locating objects specified by predefined categorical terms, such as “chair” or “refrigerator”. Methodologies in this area primarily include end-to-end approaches [3, 8, 18, 23, 27, 33], which map sensory inputs directly to action policies, and modular architectures [4–6, 11, 21, 35], which separate perception, mapping, and control into distinct subsystems. While these strategies are effective in controlled environments, they are

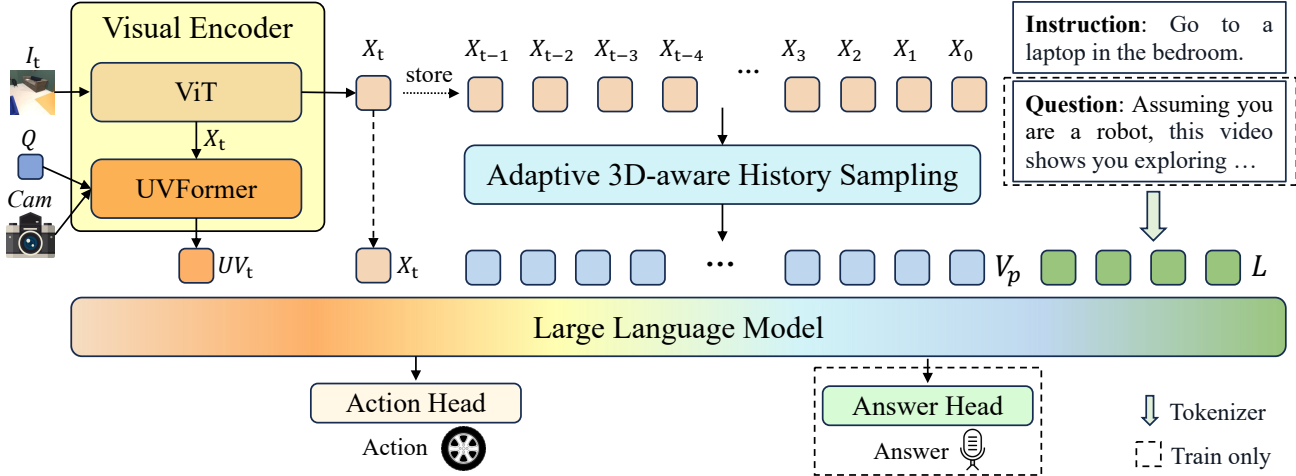


Figure 3. **Overview of P3Nav architecture.** The current frame  $I_t$  is initially processed through 2D and 3D feature extraction using the visual encoder. Then, historical features are filtered through the **Adaptive 3D-aware History Sampling** strategy. The visual features obtained, along with the accompanying linguistic instructions, are then fed into the large language model (LLM). Leveraging the **Multitask Collaboration** strategy, which significantly enhances navigation capabilities through joint training on both navigation and EQA tasks, the LLM produces two outputs via multimodal fusion: executable navigation actions and natural language answers.

limited by their reliance on a fixed set of object classes. To address these limitations, Open Vocabulary Object Goal Navigation (OVON) [29] was introduced for open-world scenarios. OVON [29] enables navigation by allowing users to describe any object using natural language, such as “find a television,” thus accommodating the diverse and dynamic nature of real-world applications. Additionally, Multi-Object Navigation (MultiON) [25] extends the task from single to multiple objects, requiring agents to navigate to a sequence of targets based on language instructions. Although current ObjectNav models are effective at finding target objects, they frequently have difficulty explaining why they chose certain paths.

## 2.2. Embodied Question Answering

EQA [7] is an innovative task where agents explore 3D environments to answer visually grounded questions, as introduced by Das et al. [7]. This multimodal challenge requires a combination of visual perception, environment exploration, and linguistic understanding. Agents must navigate physical spaces while interpreting questions, such as “What color is the car?” The EQA task was further developed by the MT-EQA dataset [30], which introduced scenarios involving multiple objects and locations, thereby increasing its complexity. Furthermore, the MP3D-EQA dataset [26] advanced the field by incorporating photorealistic environments with point cloud perception, challenging agents to interact with detailed 3D spaces. Recently, the HM-EQA dataset [20] refined exploration strategies with an “explore until confident” approach, promoting efficient data gathering for accurate decision-making. These afore-

mentioned developments collectively enhanced the capabilities of agents in EQA tasks. Building on the EQA datasets, some studies [32, 34] advance the field by unifying navigation and EQA tasks into a comprehensive model.

## 3. Methodology

In this section, we present **P3Nav**, a novel and unified framework for embodied navigation that seamlessly integrates the essential components of **Perception**, **Planning**, and **Prediction**. First, we provide an overview of P3Nav, highlighting its central component, the **Adaptive 3D-aware History Sampling** strategy, as detailed in Sec. 3.1. Then, in Sec. 3.2, we introduce an innovative method to extend navigation datasets with EQA pairs that explicitly model the decision-making processes involved in navigation. Finally, we present a **Multitask Collaboration** strategy in Sec. 3.3, which bolsters navigation capabilities by enabling joint training on both navigation and EQA tasks.

### 3.1. Model

As shown in Fig. 3, P3Net integrates three specialized components for explainable robotic navigation: a visual encoder module for current observation encoding, an adaptive 3D-aware history sampling strategy for historical context modeling, and a LLM for predicting actions and answers.

#### 3.1.1. Visual Encoder

Our visual encoder integrates 2D and 3D features to represent the current observation frame, with a dedicated emphasis on real-time perceptual cues. It consists of two special-

ized components: a ViT [19] for 2D feature extraction and UVFormer [17] for 3D spatial encoding.

First, we utilize the CLIP-pretrained ViT [19] as the image backbone for 2D feature extraction:

$$X_t = \text{ViT}(I_t), \quad (1)$$

where  $I_t \in \mathbb{R}^{H \times W \times 3}$  denotes the RGB image, and  $X_t \in \mathbb{R}^{n_{\text{img}} \times c}$  represents their corresponding 2D features at timestep  $t$ . Here,  $n_{\text{img}}$  indicates the number of image patches while  $c$  denotes the feature dimension.

Additionally, inspired by [17], we implement multi-perspective alignment through unified view projection:

$$UV_t = \text{UVFormer}(Q, X_t, \text{Cam}). \quad (2)$$

Here, the UVFormer [17] module processes three inputs: image features  $X_t$ , camera parameters  $\text{Cam}$ , and learnable queries  $Q$  that encode spatial positions and semantic features within the robot’s 3D workspace (See [17] for architectural details). The output  $UV_t \in \mathbb{R}^{n_{\text{UV}} \times c}$  aggregates multi-view visual information through a structured 3D feature volume, where  $n_{\text{UV}}$  denotes the number of 3D visual tokens. See the supplementary material for more details.

### 3.1.2. Adaptive 3D-aware History Sampling

Utilizing all observed RGB frames can substantially mitigate the issue of catastrophic knowledge forgetting, which is essential for long-term navigation. However, due to GPU memory constraints and high computational costs, storing all image features extracted from these frames is often impractical. Additionally, we have observed a significant amount of redundancy in observations during navigation, as the agent frequently revisits the same locations multiple times. To address this issue, we propose a method for selecting those frames that do not overlap in spatial positions to serve as historical features, thereby reducing observational redundancy. Furthermore, we introduce **position-enhanced historical features** that utilize the agent’s positions to augment historical semantic features with trajectory information, preventing redundant exploration of the same location.

Specifically, the adaptive 3D-aware history sampling strategy samples image features in reverse chronological order, using the spatial position of the current frame as a reference. It retains image features with relative distances beyond a defined threshold and discards those within the threshold, thus effectively minimizing redundancy and preserving essential temporal context. As shown in Algorithm 1, our adaptive 3D-aware history sampling strategy operates through three sequential phases: initialization, 3D-aware sampling, and adaptive padding.

(1) Initialization. The initialization phase (Lines 1-6) sets up the operational parameters by accepting the input parameters (current step  $t$ , window size  $W$ , threshold  $\epsilon$ ) and initializing empty buffers for historical features  $\mathbf{V}$  and relative

---

### Algorithm 1 Adaptive 3D-aware History Sampling

---

**Input:** Current step  $t$ , Window size  $W$ , Threshold  $\epsilon$

**Output:** Historical features  $\mathbf{V}$ , Relative positions  $\mathbf{P}$

```

1:  $\mathbf{V} \leftarrow \emptyset, \mathbf{P} \leftarrow \emptyset$ 
2:  $\mathbf{G} \leftarrow \text{GetAllObs}()$ 
3: if  $\mathbf{G} = \emptyset$  then
4:   # Initialize with dummy data
5:   return  $\mathbf{V}, \mathbf{P}$ 
6: end if
7: # Current frame as reference
8:  $\mathbf{p}^{\text{ref}} \leftarrow \mathbf{G}[-1].\mathbf{p}$ 
9:  $k \leftarrow 0$ 
10: # From current time  $t$  to 0
11: for  $i \leftarrow |\mathbf{G}| - 1$  to 0 do
12:    $\mathbf{p}_i^{\text{rel}} \leftarrow \mathbf{G}[i].\mathbf{p} - \mathbf{p}^{\text{ref}}$ 
13:   if  $i < |\mathbf{G}| - 1$  and  $\exists \mathbf{q} \in \mathbf{P} : \|\mathbf{p}_i^{\text{rel}} - \mathbf{q}\|_2 < \epsilon$  then
14:     # Skip redundant frames
15:     continue
16:   end if
17:    $\mathbf{V} \leftarrow \mathbf{V} \oplus \text{MaxPool}(\mathbf{G}[i].\mathbf{v})$ 
18:    $\mathbf{P} \leftarrow \mathbf{P} \oplus \mathbf{p}_i^{\text{rel}}$ 
19:    $k \leftarrow k + 1$ 
20:   if  $k = W$  then
21:     break
22:   end if
23: end for
24: while  $k < W$  do
25:   # Padding with last valid frame
26:    $\mathbf{V} \leftarrow \mathbf{V} \oplus \mathbf{V}[-1]$ 
27:    $\mathbf{P} \leftarrow \mathbf{P} \oplus \mathbf{P}[-1]$ 
28:    $k \leftarrow k + 1$ 
29: end while

```

---

positions  $\mathbf{P}$ , respectively. The *GetAllObs()* function returns all historical observations in  $\mathbf{G}$  using a First-in-First-out (FIFO) queue, where  $\mathbf{G}[0]$  corresponds to the initial time and  $\mathbf{G}[-1]$  corresponds to the current time. At time step  $i$ ,  $\mathbf{G}[i]$  includes historical features  $\mathbf{G}[i].\mathbf{v}$  paired with their corresponding agent absolute positions  $\mathbf{G}[i].\mathbf{p} = (x, y, z)$ .

(2) 3D-Aware Sampling. The core 3D-aware sampling phase (Lines 8-23) processes all historical observations in  $\mathbf{G}$  in reverse chronological order, from newest to oldest. First, it uses the robot’s absolute position  $\mathbf{p}^{\text{ref}}$  at the current step  $t$  as the spatial reference to compute relative coordinates  $\mathbf{p}_i^{\text{rel}}$  of historical features  $\mathbf{G}[i].\mathbf{v}$ . Then, using the threshold  $\epsilon$ , it dynamically filters out spatially redundant features by removing those with distances below the threshold and preserving those above to maintain critical temporal information, as described by the condition  $\|\mathbf{p}_i^{\text{rel}} - \mathbf{q}\|_2 < \epsilon$ . By adjusting the size of  $\epsilon$ , we can control the sampling density. Smaller values of  $\epsilon$  result in denser sampling, allowing more continuous historical information to be retained. Con-

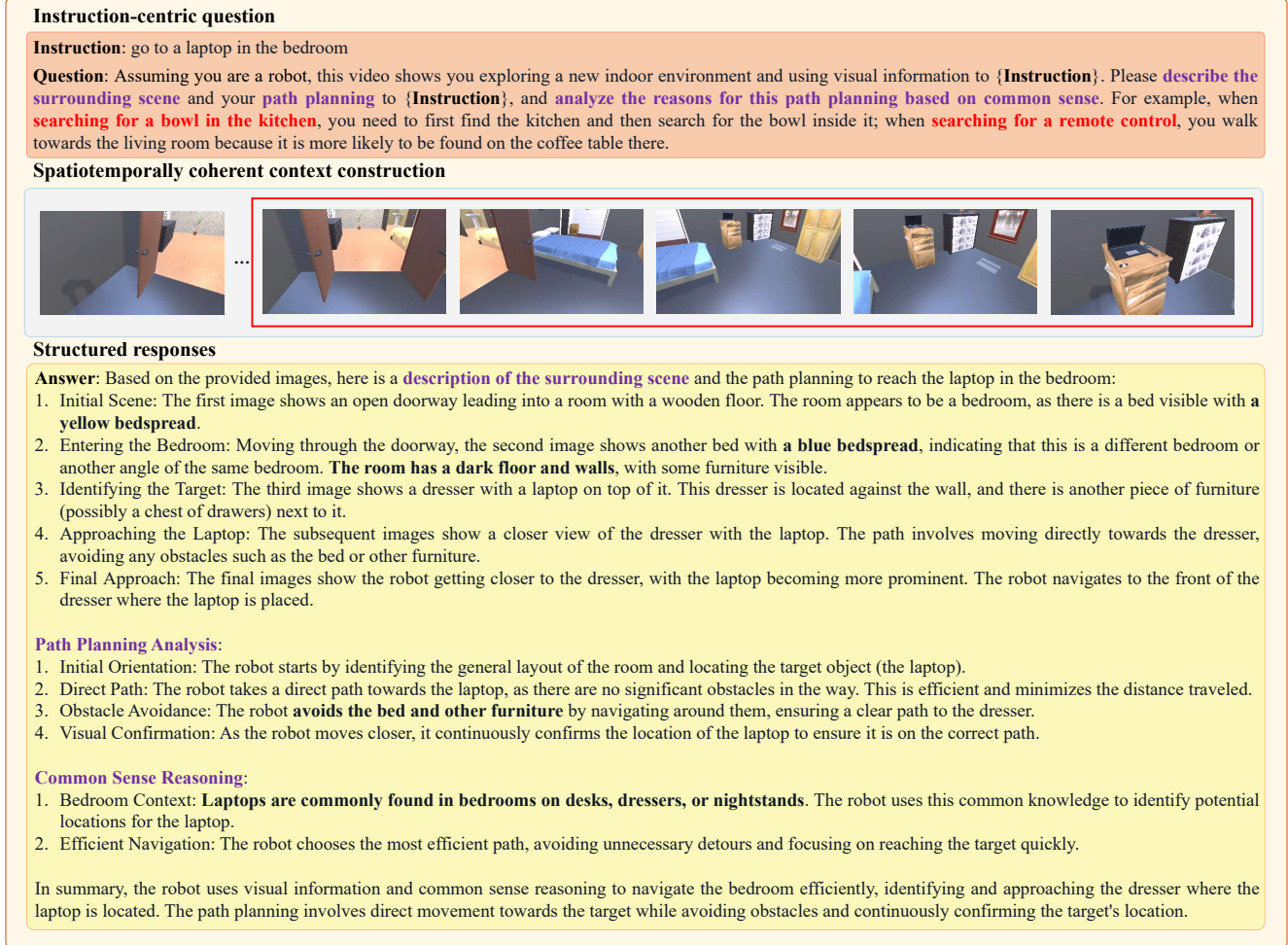


Figure 4. **EQA dataset extension framework**. The framework comprises three key stages: (1) standardized reasoning steps through instruction-centric question formulation, (2) decision context modeling via spatiotemporally coherent context construction, and (3) structured response generation integrating scene analysis, path planning, and commonsense reasoning. This hierarchical approach enables robots to systematically identify targets and formulate explainable navigation strategies while maintaining human-like decision transparency.

currently, historical features  $\mathbf{G}[i].\mathbf{v}$  undergo dimensional-reduction via a **MaxPool** operator before being stored. This phase terminates when the collected samples reach the target window size  $W$  or  $\mathbf{G}$  is empty.

(3) Adaptive Padding. The adaptive padding phase (Lines 24-28) ensures fixed-length outputs by replicating the last valid entries whenever the historical features buffer  $\mathbf{V}$  does not reach the designated window size  $W$ . Through cyclic duplication of  $\mathbf{V}[-1]$  and  $\mathbf{P}[-1]$ , it maintains temporal coherence while fulfilling model input requirements.

**Position-enhanced historical features.** For obtained historical features  $\mathbf{V}$ , positional information is critical for recording the agent's historical trajectory and planning efficient paths for future exploration. Hence, we obtain position-enhanced historical features  $\mathbf{V}_p$  by using the agents' relative positions  $\mathbf{P}$  as positional encodings for the

historical features  $\mathbf{V}$ . This integration enriches spatial semantics with 3D trajectory information, ensuring observation consistency and effectively preventing redundant exploration of previously visited locations. As agents move on the ground, their positions  $\mathbf{p}$  involve constantly changing  $x$  and  $y$  coordinates, while the  $z$  coordinate, representing height, remains constant. Consequently, we focus on encoding the agent's positions along the  $x$  and  $y$  axes to effectively capture their 3D trajectory. Inspired by the work of [24], we propose a 2D encoding through axis-separated frequency projections:

$$\omega_k = e^{-2k(\log(10000))/d}, \quad d = c/2, \quad (3)$$

$$PE_x = \left[ \sin(x\omega_{\lfloor m/2 \rfloor}), \cos(x\omega_{\lfloor m/2 \rfloor}) \right]_{m=0}^{d-1}, \quad (4)$$

$$PE_y = \left[ \sin(y\omega_{\lfloor n/2 \rfloor}), \cos(y\omega_{\lfloor n/2 \rfloor}) \right]_{n=0}^{d-1}, \quad (5)$$

$$PE(x, y) = PE_x \oplus PE_y, \quad (6)$$

where  $\oplus$  operation merges x/y-axis encodings into a unified spatial. For each element  $\mathbf{v}$  in the historical features  $\mathbf{V}$ , we calculate its position encoding  $PE(x, y)$ . By adding these features together and passing the result through a fully connected layer, we obtain the position-enhanced historical features  $\mathbf{V}_p \in \mathbb{R}^{n_{\text{his}} \times c}$  by enriching the historical features with positional information, where  $n_{\text{his}}$  denotes the number of historical features.

### 3.1.3. LLM

Finally, we integrate the position-enhanced historical features  $\mathbf{V}_p$  with the current observations  $\mathbf{UV}_t$  and  $\mathbf{X}_t$  from the visual encoder to create visual tokens for the LLM. In this framework,  $\mathbf{UV}_t$  and  $\mathbf{X}_t$  capture the agent’s ongoing environment, while  $\mathbf{V}_p$  offers context from past observations, effectively filtering out redundant positions. Similarly, input instructions or questions are transformed into language tokens  $\mathbf{L} \in \mathbb{R}^{n_L \times c}$  via a tokenizer, where  $n_L$  denotes the length of the language tokens. These visual and language tokens are combined and fed into the LLM. The LLM utilizes its abilities in multimodal alignment and comprehension to process these tokens, decoding the outputs through specialized heads. For navigation datasets, it employs an action head to generate the executable action, while for EQA datasets, it uses an answer head (i.g., LLM head) to produce the natural language answer to input questions. Please refer to the supplementary material for more details.

## 3.2. Embodied Question Answering

Current navigation models merely mimic human navigation trajectories, lacking deep thinking and task planning similar to human cognitive processes. For instance, humans typically first identify related rooms, then locate furniture, and finally search for specific objects. This lack of interpretability stems from traditional navigation datasets, which mainly focus on recording coordinate trajectories while neglecting the hierarchical reasoning used by humans. To address this issue, we have developed a new method for extending navigation datasets with EQA pairs that explicitly models the decision-making process involved in navigation.

As shown in Fig. 4, we instruct GPT-4o [12] to generate perception of the surrounding environment, navigation planning, and navigation analysis for each navigation objective. It consists of three stages: instruction-centric question, spatiotemporally coherent context construction, and structured responses.

**Instruction-centric question.** We construct an instruction-centric question that helps to generate comprehensive first-person analysis for navigation objectives (e.g., “go to a laptop in the bedroom”), through two synergistic mechanisms: role specification (“assuming you are a robot”) and exemplar-based prompting (i.e., two examples of naviga-

tion reasoning and planning, highlighted in red in Fig. 4). This dual approach ensures structured outputs that contain three essential components: (1) surrounding scene description (e.g., recognizing bedroom furniture layouts), (2) path planning analysis (e.g., creating obstacle-avoidance trajectories), and (3) common sense reasoning (e.g., prior knowledge about where laptops are typically placed).

**Spatiotemporally coherent context construction.** To ensure alignment with the adaptive 3D-aware history sampling strategy established in section 3.1.2, we systematically select the final  $W$  frames from each navigation trajectory. This frame range captures critical target-approaching phases while maintaining temporal consistency with upstream visual processing modules. By adopting this temporal window, we construct spatiotemporally coherent contexts that encode successful navigation patterns and preserve motion dynamics essential for trajectory analysis.

**Structured responses.** Building upon the prepared inputs above, we synthesize instruction-aligned multimodal prompts by combining textual question with curated visual sequences. This integration requires GPT-4o [12] to generate structured responses through three distinct reasoning phases. First, the surrounding scene description identifies architectural features (e.g., “the room has a dark floor and walls”) and object semantics (e.g., “a yellow/blue bedspread”). Second, path planning analysis devises hierarchical navigation strategies (e.g., “enter bedroom → circumvent bed → final approach”). Third, common sense reasoning incorporates human-environment interaction norms (e.g., “laptops are commonly found on desks, dressers, or nightstands”). Each phase operates sequentially, ensuring explicit alignment between perception, action planning, and contextual knowledge.

## 3.3. Multitask Collaboration

To address the limitations inherent in single-task learning, which only encompasses navigation tasks, we introduce a multitask collaboration strategy that significantly enhances navigation capabilities through joint training on both navigation and EQA tasks. As shown in Fig. 3, during the training phase, this strategy enables the model to learn from both tasks concurrently, with inputs consisting of navigational instructions and EQA questions. Consequently, the model can effectively utilize the perceptual and planning skills derived from EQA pairs to refine and improve its navigation prediction capabilities. By integrating these tasks, the model gains a comprehensive understanding of spatial relationships and decision-making processes, which are critical for accurate navigation.

In contrast, during the inference phase, the model focuses exclusively on predicting navigation actions. By maintaining this setting, the model effectively utilizes the enhanced perceptual insights and planning strategies gained

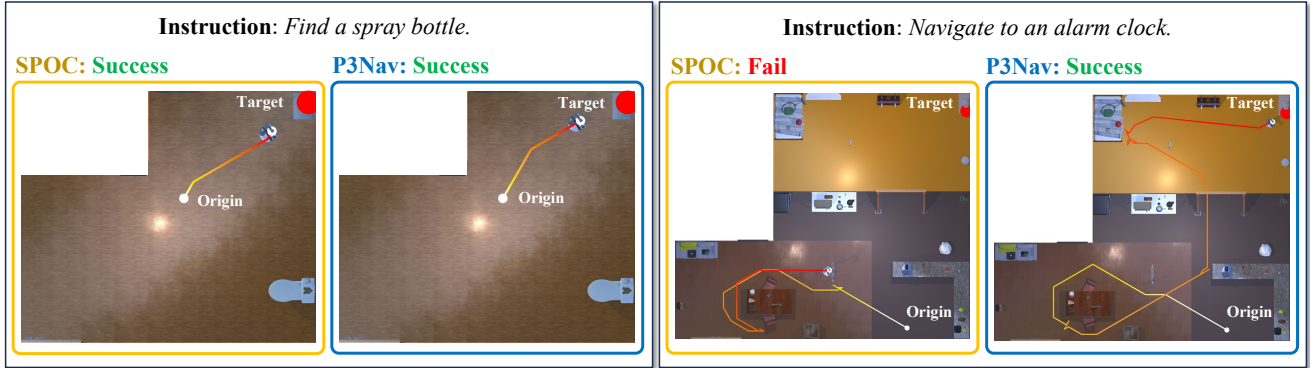


Figure 5. *Left*: Both P3Nav and SPOC [10] generate the shortest path when the agent is near the target (e.g., in the same room). *Right*: In contrast, SPOC [10] **fails** due to repeatedly searching along the same paths when distant from the target (e.g., in different rooms), whereas P3Nav **succeeds** by effectively avoiding revisiting areas and exploring new ones.

during training, enabling efficient generation of precise navigation actions. Please refer to the supplementary material for more details of training objective.

## 4. Experiments

In this section, we first outline our experimental settings, then compare our proposed method with state-of-the-art techniques, and finally provide a detailed analysis of our approach, including qualitative results and ablation studies.

### 4.1. Experimental Settings

**Dataset and Metrics.** We evaluate our proposed method on the CHORES-S ObjectNav benchmark [10]. This benchmark includes 15 object categories and annotates 99k trajectories within 10k training houses, among 5M expert trajectory frames in the AI2-THOR simulated environment [14]. Besides, we extend the navigation dataset with EQA pairs for joint training, as described in Sec. 3.2. We follow the official evaluation split of the CHORES-S ObjectNav benchmark [10], which contains 200 trajectories in 200 testing houses. To comprehensively demonstrate the effectiveness of our method, we evaluate performance using three metrics: success rate (SR), episode-length weighted success (SEL) [9], and percentage of rooms visited (%Rooms) [10]. The additional explanations of the metrics and implementation details are provided in the supplementary materials.

### 4.2. Performance Comparisons

As shown in Table 1, we compare our method with EmbSigLIP [10], SPOC [10], and SPOC\* [10]. The performance results are directly copied from the original paper or supplementary materials, with “-” indicating that the results have not been disclosed. EmbSigLIP [10] denotes an implementation of the EmbCLIP [13] model that has been upgraded to utilize the SigLIP [31] backbone, serving as a baseline model. SPOC [10] focuses on imitating shortest

Method	SR $\uparrow$	SEL $\uparrow$	%Rooms
EmbSigLIP [13]	36.5	24.5	42.2
SPOC [10]	57.0	<b>46.2</b>	51.5
SPOC* [10]	60.0	30.5	-
P3Nav	<b>75.0</b>	34.3	69.4

Table 1. Performance comparison of different navigation methods on the CHORES-S ObjectNav benchmark [10].

paths for effective navigation by modeling optimal routes. SPOC\* [10] is akin to SPOC [10], but it is trained using a larger set of expert trajectories. P3Nav integrates perception, planning, and prediction by jointly training on navigation and EQA tasks using the multitask collaboration strategy and employs the adaptive 3D-aware history sampling strategy to process historical frames.

As presented in Table 1, EmbSigLIP [13] demonstrates limited navigational performance, with the lowest SR of 36.5 and a SEL of 24.5, highlighting inefficiencies in path length. SPOC [10] shows improvement, achieving an SR of 57.0 through optimal route modeling, and obtains the highest SEL of 46.2 by focusing on shortest path learning. SPOC\* [10] further enhances SR to 60.0 via more expert trajectory training, although it results in longer paths, reducing SEL to 30.5. P3Nav utilizes adaptive 3D-aware history sampling and multitask collaboration strategies to achieve the highest SR of 75.0, effectively leveraging historical data for improved path decision-making and enhancing environmental understanding through EQA tasks. The results demonstrate that P3Nav excels in long-term navigation, surpassing other methods by integrating planning skills across both navigation and EQA tasks.

### 4.3. Qualitative Results

To further illustrate the effectiveness of our unified framework for embodied navigation, some visualization results compared with SPOC [10] are illustrated in Fig. 5. In the

Exp	HO	SP	PEHF	SR $\uparrow$	SEL $\uparrow$	%Rooms
1	✗	✗	✗	31.3	<b>16.7</b>	65.6
2	✓	✓	✗	39.2	14.4	77.7
3	✓	✗	✓	40.3	9.2	81.1
4	✓	✓	✓	<b>42.1</b>	15.2	75.0

Table 2. Ablation study on 3D-aware history sampling, where HO, SP, and PEHF stand for historical observations, sampling, and position-enhanced historical features, respectively.

left case, both P3Nav and SPOC [10] are capable of generating the shortest path when the agent is positioned close to the target, such as being in the same room. Both methods demonstrate a strong understanding of the environment, allowing them to navigate efficiently without significant difficulties. However, the right case illustrates that when the agent is farther from the target, such as in different rooms, SPOC [10] faces challenges by repeatedly searching the same paths, leading to inefficiencies in navigating complex environments. In contrast, P3Nav avoids revisiting explored areas, enabling new path exploration and enhanced navigation efficiency, thus excelling in long-term navigation.

#### 4.4. Ablation Studies

To demonstrate the effectiveness of different modules within our unified framework, we conduct ablation studies on the ObjectNavRoom benchmark [10], which has only 1/5 the sample size of ObjectNav. See the supplementary materials for more details about the ObjectNavRoom.

**Does the adaptive 3D-aware history sampling help?** We present an ablation study examining three key components, as shown in Table 2, which evaluates the impact of historical observations (HO), sampling (SP), and position-enhanced historical features (PEHF) in adaptive 3D-aware history sampling. Exp. 1, with no historical observations (i.e., window size  $W = 0$ ), focuses solely on the current visual information and achieves the lowest SR among the four experiments, highlighting the importance of historical observations for navigation. Comparing Exp. 2 and 4, we observe a 2.9 decrease in SR when position-enhanced historical features are not used, indicating that these features effectively avoid repeated exploration of the same area by adding positional information, thus enhancing navigation efficiency. Between Exp. 3 and 4, the absence of sampling in historical observations (i.e., threshold  $\epsilon = 0$ ) results in a 1.8 drop in SR, demonstrating that sampling helps improve navigation accuracy by effectively removing redundant observations.

**Does the multitask collaboration strategy help?** We conduct an ablation study on the multitask collaboration strategy to evaluate the benefits of joint training on both navigation and EQA tasks. As demonstrated in Table 3, Exp. 2, which additionally utilizes the EQA dataset during the training phase, achieves an increase of 3.0 in SR and 4.0 in

Exp	benchmark	Navigation	EQA	SR $\uparrow$	SEL $\uparrow$	%Rooms
1	ObjectNavRoom	✓	✗	42.1	15.2	75.0
2	ObjectNavRoom	✓	✓	<b>45.1</b>	<b>19.2</b>	71.9
3	ObjectNav	✓	✗	65.7	31.2	68.4
4	ObjectNav	✓	✓	<b>75.0</b>	<b>34.3</b>	69.4

Table 3. Ablation on the multitask collaboration strategy.

Exp	$W$	$\epsilon$	SR $\uparrow$	SEL $\uparrow$	%Rooms
1	20	0.1	32.6	13.2	74.8
2	40	0.1	34.8	13.0	74.7
3	60	0.1	<b>42.1</b>	15.2	75.0
4	80	0.1	38.9	<b>16.7</b>	74.3
5	100	0.1	35.2	14.3	72.3
6	60	0.05	41.5	10.3	79.9
7	60	0.15	41.3	12.6	77.8
8	60	0.2	40.5	13.7	72.1

Table 4. Analysis of different hyper-parameters for the 3D-aware history sampling strategy.

SEL compared to Exp. 1, which only employs the navigation dataset. This result indicates that integrating the EQA dataset allows agents to leverage perception and planning to improve their prediction capabilities, thereby enhancing navigation abilities. Moreover, we have identified a remarkable improvement: Exp. 4, trained on the ObjectNav benchmark, which contains five times more samples than ObjectNavRoom, exhibits a **9.3** increase in SR compared to Exp. 3. This suggests that increasing the volume of EQA data can significantly enhance navigation performance.

**On hyper-parameters.** We investigate the performance using different values of the window size  $W$  and the threshold  $\epsilon$  for the adaptive 3D-aware history sampling strategy, as they control the length of historical context and the sampling density, respectively. Through a coarse search shown in Table 4, we adopt  $W = 60$  and  $\epsilon = 0.1$  for our adaptive 3D-aware history sampling strategy.

## 5. Conclusion

In this paper, we present the **P3Nav** framework, which significantly advances language-guided visual navigation by effectively integrating **Perception**, **Planning**, and **Prediction** through **Multitask Collaboration** strategy. Additionally, P3Nav adopts an **Adaptive 3D-aware History Sampling** strategy to enhance navigation by efficiently utilizing historical data to minimize redundancy. The framework’s impressive 75% success rate in ObjectNav on the CHORES-S benchmark underscores its effectiveness. Although P3Nav has achieved remarkable results in simulated environments, there is still a long way to go to achieve truly human-like embodied navigation. Future work will address these limitations by exploring the integration of larger, more diverse datasets to further enhance P3Nav’s generalization capabilities across various environments.



## References

- [1] Peter Anderson, Angel Chang, Devendra Singh Chaplot, Alexey Dosovitskiy, Saurabh Gupta, Vladlen Koltun, Jana Kosecka, Jitendra Malik, Roozbeh Mottaghi, Manolis Savva, et al. On evaluation of embodied navigation agents. *arXiv preprint arXiv:1807.06757*, 2018. 1, 2
- [2] Anas Awadalla, Irena Gao, Josh Gardner, Jack Hessel, Yusuf Hanafy, Wanrong Zhu, Kalyani Marathe, Yonatan Bitton, Samir Gadre, Shiori Sagawa, et al. Openflamingo: An open-source framework for training large autoregressive vision-language models. *arXiv preprint arXiv:2308.01390*, 2023. 1
- [3] Tommaso Campari, Paolo Eccher, Luciano Serafini, and Lamberto Ballan. Exploiting scene-specific features for object goal navigation. In *European Conference on Computer Vision*, pages 406–421. Springer, 2020. 1, 2
- [4] Tommaso Campari, Leonardo Lamanna, Paolo Traverso, Luciano Serafini, and Lamberto Ballan. Online learning of reusable abstract models for object goal navigation. In *Proceedings of the IEEE/CVF Conference on Computer Vision and Pattern Recognition*, pages 14870–14879, 2022. 1, 2
- [5] Matthew Chang, Arjun Gupta, and Saurabh Gupta. Semantic visual navigation by watching youtube videos. *Advances in Neural Information Processing Systems*, 33:4283–4294, 2020. 1
- [6] Devendra Singh Chaplot, Dhiraj Prakashchand Gandhi, Abhinav Gupta, and Russ R Salakhutdinov. Object goal navigation using goal-oriented semantic exploration. *Advances in Neural Information Processing Systems*, 33:4247–4258, 2020. 1, 2
- [7] Abhishek Das, Samyak Datta, Georgia Gkioxari, Stefan Lee, Devi Parikh, and Dhruv Batra. Embodied question answering. In *Proceedings of the IEEE conference on computer vision and pattern recognition*, pages 1–10, 2018. 2, 3
- [8] Heming Du, Lincheng Li, Zi Huang, and Xin Yu. Object-goal visual navigation via effective exploration of relations among historical navigation states. In *Proceedings of the IEEE/CVF Conference on Computer Vision and Pattern Recognition*, pages 2563–2573, 2023. 1, 2
- [9] Ainaz Eftekhari, Kuo-Hao Zeng, Jiafei Duan, Ali Farhadi, Ani Kembhavi, and Ranjay Krishna. Selective visual representations improve convergence and generalization for embodied ai. *arXiv preprint arXiv:2311.04193*, 2023. 7, 1
- [10] Kiana Ehsani, Tanmay Gupta, Rose Hendrix, Jordi Salvador, Luca Weihs, Kuo-Hao Zeng, Kunal Pratap Singh, Yejin Kim, Winson Han, Alvaro Herrasti, et al. Spoc: Imitating shortest paths in simulation enables effective navigation and manipulation in the real world. In *Proceedings of the IEEE/CVF Conference on Computer Vision and Pattern Recognition*, pages 16238–16250, 2024. 2, 7, 8, 1, 3, 4
- [11] Saurabh Gupta, James Davidson, Sergey Levine, Rahul Sukthankar, and Jitendra Malik. Cognitive mapping and planning for visual navigation. In *Proceedings of the IEEE conference on computer vision and pattern recognition*, pages 2616–2625, 2017. 1, 2
- [12] Aaron Hurst, Adam Lerer, Adam P Goucher, Adam Perelman, Aditya Ramesh, Aidan Clark, AJ Ostrow, Akila Welihinda, Alan Hayes, Alec Radford, et al. Gpt-4o system card. *arXiv preprint arXiv:2410.21276*, 2024. 6
- [13] Apoorv Khandelwal, Luca Weihs, Roozbeh Mottaghi, and Aniruddha Kembhavi. Simple but effective: Clip embeddings for embodied ai. In *Proceedings of the IEEE/CVF Conference on Computer Vision and Pattern Recognition*, pages 14829–14838, 2022. 7
- [14] Eric Kolve, Roozbeh Mottaghi, Winson Han, Eli VanderBilt, Luca Weihs, Alvaro Herrasti, Matt Deitke, Kiana Ehsani, Daniel Gordon, Yuke Zhu, et al. Ai2-thor: An interactive 3d environment for visual ai. *arXiv preprint arXiv:1712.05474*, 2017. 7
- [15] Jacob Krantz, Erik Wijmans, Arjun Majumdar, Dhruv Batra, and Stefan Lee. Beyond the nav-graph: Vision-and-language navigation in continuous environments. In *Computer Vision—ECCV 2020: 16th European Conference, Glasgow, UK, August 23–28, 2020, Proceedings, Part XXVIII 16*, pages 104–120. Springer, 2020. 1
- [16] Alexander Ku, Peter Anderson, Roma Patel, Eugene Ie, and Jason Baldridge. Room-across-room: Multilingual vision-and-language navigation with dense spatiotemporal grounding. *arXiv preprint arXiv:2010.07954*, 2020. 1
- [17] Fanfan Liu, Feng Yan, Liming Zheng, Chengjian Feng, Yiyang Huang, and Lin Ma. Robouniview: Visual-language model with unified view representation for robotic manipulation. *arXiv preprint arXiv:2406.18977*, 2024. 4, 1
- [18] Arsalan Mousavian, Alexander Toshev, Marek Fišer, Jana Koščeká, Ayzaan Wahid, and James Davidson. Visual representations for semantic target driven navigation. In *2019 International Conference on Robotics and Automation (ICRA)*, pages 8846–8852. IEEE, 2019. 2
- [19] Alec Radford, Jong Wook Kim, Chris Hallacy, Aditya Ramesh, Gabriel Goh, Sandhini Agarwal, Girish Sastry, Amanda Askell, Pamela Mishkin, Jack Clark, et al. Learning transferable visual models from natural language supervision. In *International conference on machine learning*, pages 8748–8763. PmlR, 2021. 4, 1
- [20] Allen Z Ren, Jaden Clark, Anushri Dixit, Masha Itkina, Anirudha Majumdar, and Dorsa Sadigh. Explore until confident: Efficient exploration for embodied question answering. *arXiv preprint arXiv:2403.15941*, 2024. 3
- [21] Sohan Rudra, Saksham Goel, Anirban Santara, Claudio Gentile, Laurent Perron, Fei Xia, Vikas Sindhwani, Carolina Parada, and Gaurav Aggarwal. A contextual bandit approach for learning to plan in environments with probabilistic goal configurations. In *2023 IEEE International Conference on Robotics and Automation (ICRA)*, pages 5645–5652. IEEE, 2023. 1, 2
- [22] Manolis Savva, Abhishek Kadian, Oleksandr Maksymets, Yili Zhao, Erik Wijmans, Bhavana Jain, Julian Straub, Jia Liu, Vladlen Koltun, Jitendra Malik, et al. Habitat: A platform for embodied ai research. In *Proceedings of the IEEE/CVF international conference on computer vision*, pages 9339–9347, 2019. 2
- [23] William B Shen, Danfei Xu, Yuke Zhu, Leonidas J Guibas, Li Fei-Fei, and Silvio Savarese. Situational fusion of vi-

- sual representation for visual navigation. In *Proceedings of the IEEE/CVF international conference on computer vision*, pages 2881–2890, 2019. 1, 2
- [24] Ashish Vaswani, Noam Shazeer, Niki Parmar, Jakob Uszkoreit, Llion Jones, Aidan N Gomez, Łukasz Kaiser, and Illia Polosukhin. Attention is all you need. *Advances in neural information processing systems*, 30, 2017. 5
- [25] Saim Wani, Shivansh Patel, Unnat Jain, Angel Chang, and Manolis Savva. Multion: Benchmarking semantic map memory using multi-object navigation. *Advances in Neural Information Processing Systems*, 33:9700–9712, 2020. 3
- [26] Erik Wijmans, Samyak Datta, Oleksandr Maksymets, Abhishek Das, Georgia Gkioxari, Stefan Lee, Irfan Essa, Devi Parikh, and Dhruv Batra. Embodied question answering in photorealistic environments with point cloud perception. In *Proceedings of the IEEE/CVF Conference on Computer Vision and Pattern Recognition*, pages 6659–6668, 2019. 3
- [27] Wei Xie, Haobo Jiang, Shuo Gu, and Jin Xie. Implicit obstacle map-driven indoor navigation model for robust obstacle avoidance. In *Proceedings of the 31st ACM International Conference on Multimedia*, pages 6785–6793, 2023. 1, 2
- [28] Feng Yan, Fanfan Liu, Liming Zheng, Yufeng Zhong, Yiyang Huang, Zechao Guan, Chengjian Feng, and Lin Ma. Robomm: All-in-one multimodal large model for robotic manipulation. *arXiv preprint arXiv:2412.07215*, 2024. 1
- [29] Naoki Yokoyama, Ram Ramrakhya, Abhishek Das, Dhruv Batra, and Sehoon Ha. Hm3d-ovon: A dataset and benchmark for open-vocabulary object goal navigation. In *2024 IEEE/RSJ International Conference on Intelligent Robots and Systems (IROS)*, pages 5543–5550. IEEE, 2024. 3
- [30] Licheng Yu, Xinlei Chen, Georgia Gkioxari, Mohit Bansal, Tamara L Berg, and Dhruv Batra. Multi-target embodied question answering. In *Proceedings of the IEEE/CVF Conference on Computer Vision and Pattern Recognition*, pages 6309–6318, 2019. 3
- [31] Xiaohua Zhai, Basil Mustafa, Alexander Kolesnikov, and Lucas Beyer. Sigmoid loss for language image pre-training. In *Proceedings of the IEEE/CVF international conference on computer vision*, pages 11975–11986, 2023. 7
- [32] Jiazhao Zhang, Kunyu Wang, Shaoan Wang, Minghan Li, Haoran Liu, Songlin Wei, Zhongyuan Wang, Zhizheng Zhang, and He Wang. Uni-navid: A video-based vision-language-action model for unifying embodied navigation tasks. *arXiv preprint arXiv:2412.06224*, 2024. 3
- [33] Sixian Zhang, Xinhang Song, Weijie Li, Yubing Bai, Xinyao Yu, and Shuqiang Jiang. Layout-based causal inference for object navigation. In *Proceedings of the IEEE/CVF Conference on Computer Vision and Pattern Recognition*, pages 10792–10802, 2023. 1, 2
- [34] Duo Zheng, Shijia Huang, Lin Zhao, Yiwu Zhong, and Liwei Wang. Towards learning a generalist model for embodied navigation. In *Proceedings of the IEEE/CVF Conference on Computer Vision and Pattern Recognition*, pages 13624–13634, 2024. 3
- [35] Minzhao Zhu, Binglei Zhao, and Tao Kong. Navigating to objects in unseen environments by distance prediction. In *2022 IEEE/RSJ International Conference on Intelligent Robots and Systems (IROS)*, pages 10571–10578. IEEE, 2022. 1, 2

# P3Nav: A Unified Framework for Embodied Navigation Integrating Perception, Planning, and Prediction

## Supplementary Material

### 6. Implementation Details

In this section, we elaborate on the more detailed implementations for P3Nav in Sec. 3.

#### 6.1. Model

##### 6.1.1. Vision Encoder

Following the settings in previous works [17, 28], we input RGB images from both the head perspective  $I_t^{head}$  and the wrist perspective  $I_t^{wrist}$  into ViT [19] to obtain the 2D features  $X_t^{head}$  and  $X_t^{wrist}$ . Both  $X_t^{head}$  and  $X_t^{wrist}$  are then fed into UVFormer [17] to construct multi-view 3D features  $UV_t$ . In the navigation task, we adhere to the settings in [17, 28], utilizing only the wrist perspective  $X_t^{wrist}$  as the 2D feature  $X_t$  to broaden the exploration view. Conversely, in the EQA task, we use the head perspective  $X_t^{head}$  for the 2D feature  $X_t$  to maintain a first-person perspective, as the EQA pairs are generated from this perspective.

##### 6.1.2. LLM

We utilize OpenFlamingo [2] as our LLM, freezing the self-attention layers during training while fine-tuning the cross-attention layers. For the action head, we employ a multi-layer perceptron to map the final hidden states produced by the LLM from the  $c$ -dimensional space to the action space of the CHORES-S ObjectNav benchmark [10]. For the answer head (i.e., LLM head), we apply the *argmax* operation on the logits output by the LLM to decode the answer.

#### 6.2. Training Objective

To achieve **Multitask Collaboration**, we design a unified loss function that jointly optimizes navigation actions, question answering, and 3D occupancy through modality-specific components:

$$\mathcal{L} = \mathcal{L}_{\text{action}} + \mathcal{L}_{\text{answer}} + \lambda_{\text{occ}}\mathcal{L}_{\text{occ}}, \quad (7)$$

where  $\mathcal{L}_{\text{action}}$ ,  $\mathcal{L}_{\text{answer}}$ , and  $\mathcal{L}_{\text{occ}}$  denote navigation action prediction loss, embodied question answering loss, and 3D occupancy prediction loss respectively. The term  $\lambda_{\text{occ}}$  is the weight coefficient for the occupancy loss.

**Action prediction Loss.** We utilize behavior cloning to train the navigation model. Given an expert trajectory  $\tau = (\hat{a}_0, \dots, \hat{a}_T)$ , we use the cross-entropy loss for action prediction. The loss for the trajectory is as follows:

$$\mathcal{L}_{\text{action}} = \sum_{t=1}^T (CE(a_t, \hat{a}_t)), \quad (8)$$

where  $a_t$  denotes the predicted action and  $\hat{a}_t$  the ground-truth (GT) demonstration at timestep  $t$ .

**Question answering loss.** Given the GT answer  $y_{1:K}$  of the input question with the length of  $K$ , we optimize the generated answer token probabilities by a conventional cross-entropy loss:

$$L_{\text{answer}} = - \sum_{k=1}^K \log(p(y_k | y_{1:k-1})). \quad (9)$$

**Occupancy loss.** Following the approach used in previous works [17, 28], we utilize a standard cross-entropy loss function, denoted as  $L_{\text{occ}}$ , on the generated 3D volume.

### 7. Experimental Settings

#### 7.1. Dataset and Metrics

##### 7.1.1. Dataset

For the CHORES-S ObjectNav benchmark [10], we extend each trajectory with EQA pairs. As a result, we collect 99k EQA pairs as the corresponding EQA dataset for joint training. The CHORESNAV-S ObjectNavRoom benchmark [10] is similar to the ObjectNav benchmark but involves smaller trajectories. This benchmark includes 15 object categories and annotates 21k trajectories within 2k training houses out of 1M expert trajectory frames. Additionally, the ObjectNavRoom benchmark uses more diverse instructions, describing both the object’s category and its room type simultaneously, such as “Find a vase in the living room.” In contrast, the ObjectNav benchmark specifies only the object’s category, such as “Find a vase.” Similarly, we extend each trajectory in the ObjectNavRoom benchmark with EQA pairs, collecting 21k EQA pairs as the corresponding EQA dataset for ablation studies.

The action space of the ObjectNav and ObjectNavRoom benchmarks [10] includes 20 actions: Move Base ( $\pm 20$  cm); Rotate Base ( $\pm 6^\circ$ ,  $\pm 30^\circ$ ); Move Arm ( $x$ ,  $z$ ) ( $\pm 2$  cm,  $\pm 10$  cm); Rotate Grasper ( $\pm 10^\circ$ ); pickup; dropoff; done with subtask; and terminate.

##### 7.1.2. Metrics

**Success rate (SR)** is defined as the proportion of episodes deemed successful, which occurs when the agent executes the “end” action and the distance to the target, any instance of the category, is within a specified threshold (e.g.,  $2m$ ).

**Episode-length weighted success (SEL)** [9] is a metric used to evaluate the efficiency of an agent’s navigation. It

compares the shortest possible path to the agent’s actual path, calculated as:

$$\frac{1}{N} \sum_{i=1}^N S_i \frac{w_i}{\max(w_i, e_i)}, \quad (10)$$

where  $w_i$  represents the shortest possible episode length to the target object,  $e_i$  is the episode length produced by the agent, and  $S_i$  is a binary indicator that denotes success for episode  $i$ . **Percentage of rooms visited (%Rooms)** is a metric that measures the proportion of distinct rooms an agent successfully visits during navigation relative to the total number of rooms available in the environment. This metric reflects the agent’s exploratory capability and efficiency in covering different areas within a given space.

## 7.2. Traing Strategy

Here, we describe the model hyper-parameters and training details of P3Nav.

### 7.2.1. Model Hyper-parameters

In the visual encoder, the number of image patches  $n_{\text{img}}$  is set to 64, the number of multi-view vision tokens  $n_{\text{uv}}$  is 400, and the feature dimension  $c$  is 1024. In the adaptive 3D-aware history sampling strategy, the window size  $W$  is 60, the proximity threshold  $\epsilon$  is 0.1, and the number of historical frames  $n_{\text{his}}$  is 60. For the **MaxPool** operator, we use an adaptive max pooling function to reduce the number of tokens in the historical features  $\mathbf{G}[i].\mathbf{v}$  to 1. In the LLM, the number of language tokens  $n_{\text{L}}$  corresponds to the length of input instructions and questions, respectively.

### 7.2.2. Training Details

We train the entire model with the AdamW optimizer using 8 A100 GPUs (80 GB memory per GPU), with a batch size of 48 per GPU, resulting in a total batch size of 384 for 5 epochs. A cosine learning rate strategy is employed, where the learning rate is initially set to  $1 \times 10^{-4}$  and finally decays to  $1 \times 10^{-6}$ . We evaluate checkpoints every 0.5 epoch starting from the 3rd epoch and report the metrics for the checkpoint with the highest SR on the evaluation split.

## 8. Qualitative Results

To visualize the effectiveness of our unified framework for embodied navigation, we provide additional qualitative results generated by our method alongside those of SPOC [10]. As shown in Fig.6, when the agent is positioned close to the target, such as within the same room, our P3Nav is capable of generating the shortest path comparable to SPOC [10]. Both methods understand the environment well, enabling efficient navigation under familiar conditions. However, when the agent needs to navigate across greater distances, such as being situated in different rooms

from the target, significant differences in their performance begin to emerge. As shown in Fig. 7, SPOC [10] struggles by repeating paths, which reduces efficiency and increases the risk of looping or missing optimal routes, lowering its success rate. In contrast, P3Nav avoids revisiting areas, systematically explores new routes, and adapts to changing environments, making it effective for long-distance navigation and optimizing complex pathways.

**Instruction:** *Find a toilet.*

**SPOC**



**P3Nav**

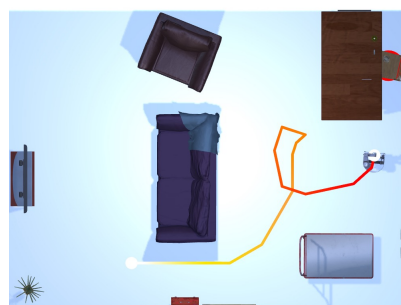


**Instruction:** *Locate a chair.*

**SPOC**

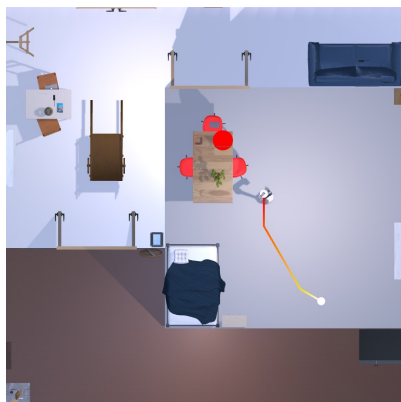


**P3Nav**



**Instruction:** *Find a laptop.*

**SPOC**



**P3Nav**

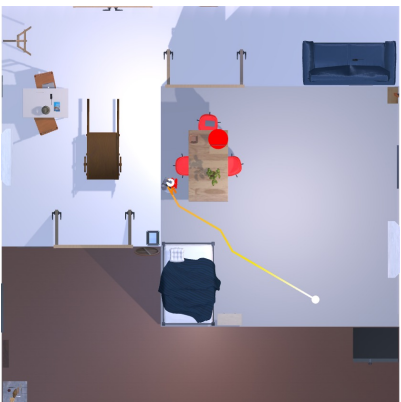
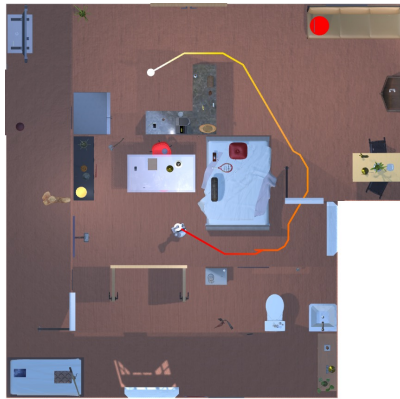


Figure 6. Qualitative comparison of trajectories generated by SPOC [10] and P3Nav in the same room.

**Instruction:** *Find a laptop.*

**SPOC**



**P3Nav**



**Instruction:** *Locate a chair.*

**SPOC**

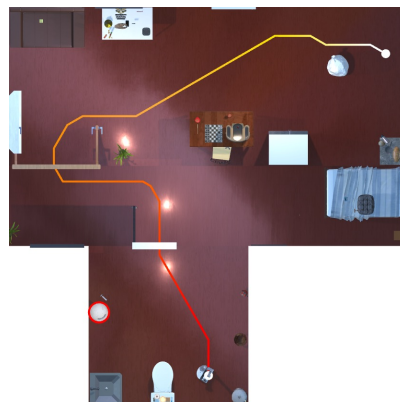


**P3Nav**



**Instruction:** *Locate a trash can.*

**SPOC**



**P3Nav**

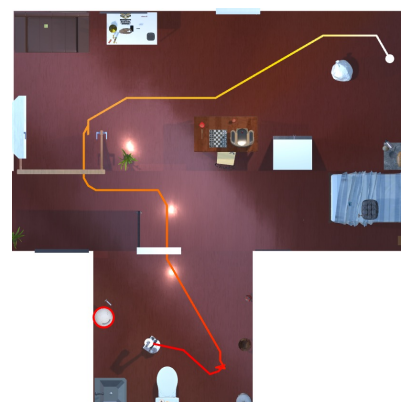


Figure 7. Qualitative comparison of trajectories generated by SPOC [10] and P3Nav in different rooms.